# Efficient Finite Element Modelling and Simulation of Gas and Fluid Supported Membrane and Shell Structures

T. Rumpel, K. Schweizerhof and M. Haßler[1]

Institute of Mechanics, University Karlsruhe (TH), Kaiserstr. 12, 76128 Karlsruhe, Germany, Karl.Schweizerhof@bau-verm.uni-karlsruhe.de

**Summary.** In statics, the large deformation analysis of membrane or shell structures loaded and/or supported by gas or fluid can be based on a finite element description for the structure only. Then in statics the effects in the gas or the fluid have to be considered by using the equations of state for the gas or the fluid, the information about the current volume and the current shape of the structure. The interaction of the gas/fluid with the structure, which can be also otherwise loaded, is then modelled by a pressure resulting from the gas/fluid always acting normal to the current wetted structural part. This description can be also directly used to model slow filling processes without all the difficulties involved with standard discretization procedures. In addition the consistent derivation of the nonlinear formulation and the linearization for a Newton type scheme results in a particular formulation which can be cast into a very efficient solution procedure based on a sequential application of the Sherman-Morrison formula. The numerical examples show the efficiency and the effects of the developed algorithms which are particularly important for structures, where the volume of the gas of fluid has to be considered.

**Key words:** Pressure loading, hydrostatics, large deformations, finite elements, deformation dependent loading, membranes, shell structures

## 1 Introduction

The simulation of the inflation resp. filling and the support of thin membrane or shell type structures by gas or fluids can be usually performed in an efficient way by assuming an internal pressure in the structure which acts normal to the inner surface [2], [3], [12] besides any other loading. The restriction of this model is that it does not take into account the change of the volume of the gas or fluid due to the deformation of the structure even if there is no further inflation or filling. Also the pressure may change due to temperature modifications of the gas/fluid. In both cases the volume of the gas resp. the mass conservation of the fluid has to be considered in the model [1], [7]; this



*E. Oñate and B. Kröplin (eds.), Textile Composites and Inflatable Structures*, 153–172.

is also important for stability considerations of the gas/fluid filled structure under any other external loading. Then in the case of gas filling the internal gas pressure formally provides an additional rank-one update of the FE stiffness matrix which stabilizes from an engineering point of view an almost completely flexible structure. Hydrostatics with a free fluid surface, also leads to an additional rank-one update of the FE stiffness matrix, whereas compressible, heavy fluids lead to a rank-two update [5].

Thus in the case of fluid filling [6], [8], [10] or a mixture of gas and fluid [9] the filling of membrane-like structures can be performed without a separate discretization of the fluid with e.g. FE or Finite Volumes or similar. Also fully fluid filled structures can be analyzed without separate discretization of the fluid [9]. Several cases have to be distinguished, fluid with a free surface [8], [10], structure under overpressure of fluid [9] and fluid with free surface but gas overpressure. The contribution shows the derivation of the variational formulation and the corresponding Finite Element discretization for compressible fluids under gravity loading. A particular focus is on the consistent linearization of the nonlinear equations and the accompanying constraint equations. Also the specific solution of the linearized equation system based on a sequential application of the Sherman-Morrison formula is presented. The numerical examples show large deformation analyses of gas and fluid filled shell structures with rather thin flexible walls under various conditions, such as filling and loading.

## 2 Governing Equations

The mathematical description of static fluid structure interaction can be based on the principle of stationarity for the total potential energy $\delta W$ of a fluid in an elastic structure and additional equations describing the physical behavior of different fluids or gases.

### 2.1 Virtual Work Expression

The variation of the elastic potential of the structure is specified by $\delta^{el}V$, $\delta^{i}\Pi$ denotes the virtual work of the pressure loading which acts between the fluid $i$ and the structure, $\delta^{ex}\Pi$ is the virtual work of other external forces acting on the structure

$$\delta W = \delta^{el}V + \delta^{i}\Pi - \delta^{ex}\Pi = 0 \tag{1}$$

The interaction term between fluid and structure is described by a body fixed pressure force ${}^{i}p\ {}^{*}\mathbf{n}$, with a non-normalized normal vector ${}^{*}\mathbf{n} = \mathbf{e}_{\xi} \times \mathbf{e}_{\eta}$ and the pressure level ${}^{i}p$, see equation (2). $\mathbf{e}_{\xi} = \frac{\partial x}{\partial \xi}$, $\mathbf{e}_{\eta} = \frac{\partial x}{\partial \eta}$ denote covariant non-normalized vectors on the wetted surface of the structure

$$\delta^{i}\Pi = \int_{\eta}\int_{\xi} {}^{i}p\ {}^{*}\mathbf{n} \cdot \delta\mathbf{u}\ d\xi d\eta \tag{2}$$

The pressure acts normal to the surface element $d\xi d\eta$ along the virtual displacement $\delta\mathbf{u}$. Therefore a virtual work expression of a follower force is given. Possible physical properties of the fluid $i$ are summarized in the following paragraphs:

### 2.2 Compressible Fluids

If the dead weight of a fluid is neglected, we can distinguish between a pneumatic model, see [1], [7] and a hydraulic description. The corresponding constitutive equations are the Poisson's law for a pneumatic ($i = p$) and the Hooke's law ($i = h$) for a hydraulic model.

#### Pneumatic Model

In realistic physical situations the investigations can be restricted to conservative models, which entails the application of the adiabatic state equation

$$^{p}p\ v^{\kappa} = \ ^{p}P\ V^{\kappa} = const. \tag{3}$$

$^{p}p,\ v$ are the state variables (pressure and volume) of the gas in the deformed state, capital letters denote the initial state and $\kappa$ the isentropy constant.

#### Hydraulic Model

For an analysis of hydraulic systems the fluid pressure is given by Hooke's law. $^{h}p$ is the mean pressure in the fluid determined by the bulk modulus $K$ and the relative volume change of the fluid with $V$ as initial volume

$$^{h}p(v) = -K\frac{v-V}{V} \tag{4}$$

### 2.3 Hydrostatic Loading – Incompressible Fluids under Gravity Loading

For partially filled structures the liquid can be treated as incompressible, see [6], [8], [10]. The pressure distribution is given by the hydrostatic pressure law, with $\rho$ as the constant density, $\mathbf{g}$ as the gravity and with the difference of the upper liquid level $^{o}\mathbf{x}$ and an arbitrary point $\mathbf{x}$ on the wetted structure. A conservative description is achieved, if the volume conservation of the liquid is taken into account during the deformation of liquid and structure, too

$$^{g}p = \rho\mathbf{g}\cdot(^{o}\mathbf{x}-\mathbf{x}) \tag{5}$$

$$\text{and} \qquad v = const. \tag{6}$$

### 2.4 Compressible Hydrostatic Loading – Compressible Fluids Under Gravity Loading

A further important case is the composition of dead weight and compressibility of fluid ($i = hg$), see [5],[9]. The corresponding pressure law for technical applications can be found by combining Hooke's law and mass conservation with the assumption of an uniform density distribution throughout the fluid. The hydrostatic pressure law for compressible fluids can be derived from a variational analysis of the gravity potential and the virtual work expression of the pressure resulting from Hooke's law

$$ {}^{hg}p = {}^{c}p - {}^{x}p - {}^{h}p \tag{7} $$

$$ = \rho(v)\mathbf{g} \cdot (\mathbf{c} - \mathbf{x}) - {}^{h}p \tag{8} $$

$$ \text{with} \quad \rho(v)v = const. \tag{9} $$

${}^{c}p = \rho(v)\mathbf{g} \cdot \mathbf{c}$ is the pressure at the center $\mathbf{c}$ of volume, ${}^{x}p = \rho(v)\mathbf{g} \cdot \mathbf{x}$ denotes the pressure at an arbitrary point $\mathbf{x}$ on the wetted structure. In the view of a mesh-free representation of the fluid, the constitutive equations are dependent on the shape and on the volume of the gas or fluid enclosed by the structure or by parts of the structure. It must be noted that the term ${}^{c}p$ is responsible for the compression of the fluid due to its own dead weight.

### 2.5 Boundary Integral Representation of Volume and Center of Volume

The goal of this approach is that all necessary quantities can be expressed by a boundary integral representation. This allows to formulate all state variables via an integration of the surrounding wetted surface. The fluid volume $v$ and the center $\mathbf{c}$ of the volume can be computed via:

$$ v = \frac{1}{3} \int_{\eta} \int_{\xi} \mathbf{x} \cdot^{*} \mathbf{n} \; d\xi d\eta \tag{10} $$

$$ \text{and} \quad \mathbf{c} = \frac{1}{4v} \int_{\eta} \int_{\xi} \mathbf{x} \; \mathbf{x} \cdot^{*} \mathbf{n} \; d\xi d\eta \tag{11} $$

A large deformation analysis of the structure including the fluid can be performed using a Newton type scheme for the solution by applying a Taylor series expansion on the governing equations. The following linearization is shown in short for all four cases discussed above. For details we refer to [1], [6], [7].

## 3 Linearization of the Volume Contribution for Gas and Fluid Models

Within the Newton scheme the deformed state is computed iteratively. Both, the virtual expression and the different additional constraint equations have to be consistently linearized. The linearization of the virtual work expression leads always to three parts, the residual part $\delta^{phg}\Pi_t$, the follower force part $\delta^{phg}\Pi^{\Delta n}$ and the pressure level part $\delta^{phg}\Pi^{\Delta p}$

$$\delta^{phg}\Pi_{lin} = \delta^{phg}\Pi_t + \delta^{phg}\Pi^{\Delta n} + \delta^{phg}\Pi^{\Delta p} \tag{12}$$

$$= \int_\eta \int_\xi ({}^{phg}p_t\ {}^*\mathbf{n}_t + {}^{phg}\ p_t \Delta^*\mathbf{n} + \Delta^{phg}p^*\mathbf{n}_t) \cdot \delta\mathbf{u}\ d\xi d\eta. \tag{13}$$

## 3.1 Pneumatic and Hydraulic Model

The follower force part is dependent on the structural displacements $\Delta\mathbf{u}$ respectively the change of the non-normalized normal ${}^*\mathbf{n}$, and thus indirectly on the size of the wetted surface with

$$\Delta^*\mathbf{n} = \Delta\mathbf{u},_\xi \times \mathbf{x}_t,_\eta + \mathbf{x}_t,_\xi \times \Delta\mathbf{u},_\eta\,. \tag{14}$$

The pressure change differs only slightly for both models and is only dependent on the volume change

$$\textbf{pneumatic model:}\quad \Delta^p p = -\kappa \frac{p_t}{v_t} \int_\eta \int_\xi {}^*\mathbf{n}_t \cdot \Delta\mathbf{u}\ d\xi d\eta \tag{15}$$

$$\textbf{hydraulic model:}\quad \Delta^h p = -\frac{K}{V} \int_\eta \int_\xi {}^*\mathbf{n}_t \cdot \Delta\mathbf{u}\ d\xi d\eta \quad \text{with } V \equiv v_0 \tag{16}$$

Introducing both into (13) and integrating by parts, we obtain a field and boundary valued problem. The boundary value part vanishes completely for closed structures respectively the parts enclosing the gas/fluid volume. Thus the linearized virtual expression reads:

$$\begin{aligned}
\delta^{p,h}\Pi_{lin} &= \delta^{p,h}\Pi_t \\
&\quad - \kappa \frac{p_t}{v_t} \int_\eta \int_\xi \delta\mathbf{u} \cdot^* \mathbf{n}_t\ d\xi d\eta \int_\eta \int_\xi {}^*\mathbf{n}_t \cdot \Delta\mathbf{u}\ d\xi d\eta \qquad \text{pneumatic} \\
&\quad - \frac{K}{V} \int_\eta \int_\xi \delta\mathbf{u} \cdot^* \mathbf{n}_t\ d\xi d\eta \int_\eta \int_\xi {}^*\mathbf{n}_t \cdot \Delta\mathbf{u}\ d\xi d\eta \qquad \text{hydraulic} \\
&\quad + \frac{{}^{p,h}p_t}{2} \int_\eta \int_\xi \begin{pmatrix} \delta\mathbf{u} \\ \delta\mathbf{u},_\xi \\ \delta\mathbf{u},_\eta \end{pmatrix} \cdot \begin{pmatrix} 0 & \underline{\mathbf{W}}^\xi & \underline{\mathbf{W}}^\eta \\ \underline{\mathbf{W}}^{\xi T} & 0 & 0 \\ \underline{\mathbf{W}}^{\eta T} & 0 & 0 \end{pmatrix} \begin{pmatrix} \Delta\mathbf{u} \\ \Delta\mathbf{u},_\xi \\ \Delta\mathbf{u},_\eta \end{pmatrix} d\xi d\eta
\end{aligned} \tag{17}$$

with the skew symmetric tensors

$$\underline{\mathbf{W}}^\xi =^* \mathbf{n}_t \otimes \mathbf{e}^\xi - \mathbf{e}^\xi \otimes^* \mathbf{n}_t \underline{\mathbf{W}}^\eta =^* \mathbf{n}_t \otimes \mathbf{e}^\eta - \mathbf{e}^\eta \otimes^* \mathbf{n}_t. \tag{18}$$

Obviously the final linearized expression is a symmetric displacement formulation indicating that the proposed model is conservative as expected.

### 3.2 Hydrostatic Loading – Incompressible Fluids Under Gravity Loading

The follower force part depends as in 3.1 from the change in the normal and of the gradient of the fluid under gravity loading. The latter comes into the formulation after partial integration resulting in

$$\begin{aligned}\delta^g \Pi_{lin}^{\Delta n} &= \frac{\rho}{2}\int_\eta \int_\xi \delta\mathbf{u}\cdot\left[\mathbf{g}\cdot\mathbf{e}_\xi \underline{\mathbf{W}}^\xi + \mathbf{g}\mathbf{e}_\eta \underline{\mathbf{W}}^\eta\right] \Delta\mathbf{u}\; d\xi d\eta \\ &+ \int_\eta \int_\xi \frac{{}^g p_t}{2} \begin{pmatrix}\delta\mathbf{u}\\ \delta\mathbf{u},_\xi \\ \delta\mathbf{u},_\eta\end{pmatrix} \cdot \begin{pmatrix} 0 & \underline{\mathbf{W}}^\xi & \underline{\mathbf{W}}^\eta \\ \underline{\mathbf{W}}^{\xi T} & 0 & 0 \\ \underline{\mathbf{W}}^{\eta T} & 0 & 0\end{pmatrix} \begin{pmatrix}\Delta\mathbf{u}\\ \Delta\mathbf{u},_\xi \\ \Delta\mathbf{u},_\eta\end{pmatrix} d\xi d\eta. \end{aligned} \tag{19}$$

It is obvious that the first part is non-symmetric and disappears if $\mathbf{g}$ is set to zero. The interesting part is the volume conservation and its influence on the pressure in the linearized form. The linearized pressure is a function of the variation of the fluid level $\Delta^0\mathbf{u}$ and the local structural deformation $\Delta\mathbf{u}$

$$\Delta^g p = \rho\mathbf{g}\cdot(\Delta^o\mathbf{u} - \Delta\mathbf{u}). \tag{20}$$

The volume change is zero thus the linearization is zero as well:

$$\Delta^g v = \int_\eta \int_\xi {}^*\mathbf{n}_t \cdot \Delta\mathbf{u}\; d\xi d\eta + \int_{{}^o\eta}\int_{{}^o\xi} {}^o\mathbf{n}_t \cdot \Delta^o\mathbf{u}\; d^o\xi d^o\eta = 0. \tag{21}$$

Focusing on the fluid load part – the second part in (21) – we obtain based on the direction of the normal on the fluid level, which is identical to the direction of gravity, the components of the free fluid surface and the corresponding displacement

$${}^o n_t = {}^o\mathbf{n}_t \cdot \frac{\mathbf{g}}{|\mathbf{g}|}, \tag{22}$$

$$\Delta^o u = \Delta^o\mathbf{u}\cdot\frac{\mathbf{g}}{|\mathbf{g}|}. \tag{23}$$

Thus the volume change due to the change in the fluid level can be written as

$$\Delta^o v = \int_{{}^o\eta}\int_{{}^o\xi} {}^o\mathbf{n}_t \cdot \frac{\mathbf{g}}{|\mathbf{g}|}\Delta^o\mathbf{u}\cdot\frac{\mathbf{g}}{|\mathbf{g}|}\; d^o\xi d^o\eta. \tag{24}$$

Obviously both quantities in the integral are scalars; in addition the fluid level displacement is uniform, thus we obtain

$$\Delta^o v = \Delta^o u \int_{{}^o\eta}\int_{{}^o\xi} {}^o\mathbf{n}_t \cdot \frac{\mathbf{g}}{|\mathbf{g}|}\; d^o\xi d^o\eta = \Delta^o u S_t. \tag{25}$$

$S_t$ is the size of the water surface, which can also be computed via a boundary integral over the enclosure of the fluid volume projected onto the direction of gravity

$$S_t = \int_\eta \int_\xi {}^*\mathbf{n}_t \cdot \frac{\mathbf{g}}{|\mathbf{g}|} \, d\xi d\eta. \tag{26}$$

Thus the change in the water level height can be written as

$$\Delta^o u = \frac{\Delta^o v}{S_t} = \frac{1}{S_t} \int_\eta \int_\xi {}^*\mathbf{n}_t \cdot \Delta\mathbf{u} \, d\xi d\eta \tag{27}$$

and the corresponding pressure change becomes

$$\begin{aligned} \Delta p &= \rho \mathbf{g} \cdot \Delta^o \mathbf{u} - \rho \mathbf{g} \cdot \Delta\mathbf{u} \\ &= \rho \frac{|\mathbf{g}|}{S_t} \int_\eta \int_\xi {}^*\mathbf{n}_t \cdot \Delta\mathbf{u} \, d\xi d\eta - \rho \mathbf{g} \cdot \Delta\mathbf{u}. \end{aligned} \tag{28}$$

The linearized variational form of the gravity potential depending on the fluid level is then obtained as

$$\begin{aligned} \delta^g \Pi_{lin}^{\Delta p} &= \int_\eta \int_\xi \Delta p^* \mathbf{n}_t \cdot \delta\mathbf{u} \, d\xi d\eta \\ &= \rho \frac{|\mathbf{g}|}{S_t} \int_\eta \int_\xi \delta\mathbf{u} \cdot^* \mathbf{n}_t \, d\xi d\eta \int_\eta \int_\xi {}^*\mathbf{n}_t \cdot \Delta\mathbf{u} \, d\xi d\eta \\ &\quad -\rho \int_\eta \int_\xi \delta\mathbf{u} \cdot^* \mathbf{n}_t \; \mathbf{g} \cdot \Delta\mathbf{u} \, d\xi d\eta. \end{aligned} \tag{29}$$

Obviously the second part of this equation is a non-symmetric term. However, combining both non-symmetric parts of $\delta^g \Pi_{lin}^{\Delta n}$ and $\delta^g \Pi_{lin}^{\Delta p}$, a symmetric expression results for the complete sum

$$\begin{aligned} \delta^g \Pi_{lin} &= \delta^g \Pi_{lin}^{\Delta n} + \delta^g \Pi_{lin}^{\Delta p} + \delta^g \Pi_t \\ &= \delta^g \Pi_t + \\ &\quad + \rho \frac{|\mathbf{g}|}{S_t} \int_\eta \int_\xi \delta\mathbf{u} \cdot {}^*\mathbf{n}_t \, d\xi d\eta \int_\eta \int_\xi {}^*\mathbf{n}_t \cdot \Delta\mathbf{u} \, d\xi d\eta \qquad \text{Term I} \\ &\quad - \frac{\rho}{2} \int_\eta \int_\xi \delta\mathbf{u} \cdot ({}^*\mathbf{n}_t \otimes \mathbf{g} + \mathbf{g} \otimes {}^*\mathbf{n}_t) \Delta\mathbf{u} \, d\xi d\eta \qquad \text{Term II} \\ &\quad + \int_\eta \int_\xi \frac{{}^g p_t}{2} \begin{pmatrix} \delta\mathbf{u} \\ \delta\mathbf{u}_{,\xi} \\ \delta\mathbf{u}_{,\eta} \end{pmatrix} \cdot \begin{pmatrix} 0 & \underline{\mathbf{W}}^\xi & \underline{\mathbf{W}}^\eta \\ \underline{\mathbf{W}}^{\xi T} & 0 & 0 \\ \underline{\mathbf{W}}^{\eta T} & 0 & 0 \end{pmatrix} \begin{pmatrix} \Delta\mathbf{u} \\ \Delta\mathbf{u}_{,\xi} \\ \Delta\mathbf{u}_{,\eta} \end{pmatrix} d\xi d\eta. \\ &\qquad \text{Term III} \end{aligned} \tag{30}$$

### 3.3 Compressible Fluids Under Gravity

Considering only the gravity potential of a compressible fluid, we have to integrate over the total volume of the fluid

$$^{hg}\Pi = -\int_v \rho(\mathbf{x})\mathbf{g}\cdot\mathbf{x}dv + \text{const.} \tag{31}$$

In general the density $\rho(\mathbf{x})$ is dependent on the height of the fluid, however, for technical applications with standard heights the density can be assumed to be given by the law of mass conservation. Then for compressible and incompressible fluids the potential is only a function of the form and the volume of the enclosed fluid

$$^{hg}\Pi = -\rho(v)\int_v \mathbf{g}\cdot\mathbf{x}dv + \text{const.} \tag{32}$$

This can be written as a surface integral

$$\begin{aligned} ^{hg}\Pi &= -\rho(v)\int_\eta\int_\xi \ \mathbf{g}\cdot\mathbf{x}\ \mathbf{x}\cdot{}^{*}\ \mathbf{n}\ d\xi d\eta + \text{const.} \\ &= -\rho(v)\mathbf{g}\cdot\mathbf{s}\ , \qquad \mathbf{s}\text{: 1.order volume moment} \end{aligned} \tag{33}$$

The corresponding linearized functional contains two major parts:

$$\delta^{hg}\Pi_{lin} = -\delta\rho(v)\mathbf{g}\cdot\mathbf{s} - \rho(v)\mathbf{g}\cdot\delta\mathbf{s}. \tag{34}$$

From mass conservation $\rho(v)v = \rho_o V$ with $\rho_o, V$ as reference values, we obtain

$$\delta\rho(v) = -\rho_o\frac{V}{v^2}\delta v = -\frac{\rho(v)}{v}\delta v \tag{35}$$

with

$$\delta v = \int_\eta\int_\xi \ {}^{*}\mathbf{n}\cdot\delta\mathbf{u}\ d\xi d\eta. \tag{36}$$

The variation of the second part is identical to the variation shown in the previous paragraph. After defining the location of the center of gravity of the fluid

$$\mathbf{c} = \frac{\mathbf{s}}{v}, \tag{37}$$

the variation follows as

$$\delta^{hg}\Pi = \rho(v)\int_\eta\int_\xi \mathbf{g}\cdot(\mathbf{c}-\mathbf{x})\ {}^{*}\mathbf{n}\cdot\delta\mathbf{u}\ d\xi d\eta. \tag{38}$$

Introducing the compressibility of the fluid in an identical fashion as in 3.1 with Hooke's law

$$^{h}p(v) = -K\frac{v-V}{V}, \tag{39}$$

the final term of a compressible fluid is given as

$$\delta^{hg}W = \ {}^{hg}p(v) \int_\eta \int_\xi {}^{*}\mathbf{n} \cdot \delta\mathbf{u} \ d\xi d\eta. \tag{40}$$

It is of some help to subdivide the pressure into three parts, ${}^{h}p(v)$ as above and

$$ {}^{x}p = \rho(v)\mathbf{g} \cdot \mathbf{x}, \tag{41}$$

$$ {}^{c}p = \rho(v)\mathbf{g} \cdot \mathbf{c}. \tag{42}$$

Then the form shown in (7) is given and linearization is a straightforward process with

$$\Delta^{hg}p = \Delta^{c}p - \Delta^{x}p - \Delta^{h}p \tag{43}$$

$$\Delta^{c}p = -2\frac{{}^{c}p_t}{v_t} \int_\eta \int_\xi {}^{*}\mathbf{n}_t \cdot \Delta\mathbf{u} \ d\xi d\eta + \int_\eta \int_\xi \frac{{}^{x}p_t}{v_t} \ {}^{*}\mathbf{n}_t \cdot \Delta\mathbf{u} \ d\xi d\eta \tag{44}$$

$$\Delta^{x}p = -\frac{{}^{x}p_t}{v_t} \int_\eta \int_\xi {}^{*}\mathbf{n}_t \cdot \Delta\mathbf{u} \ d\xi d\eta + \rho_t \mathbf{g} \cdot \Delta\mathbf{u} \tag{45}$$

$$\Delta^{h}p = -\frac{K}{V} \int_\eta \int_\xi {}^{*}\mathbf{n}_t \cdot \Delta\mathbf{u} \ d\xi d\eta \tag{46}$$

The summary of the pressure changes introduced into the linearized virtual work expression results in a symmetric displacement formulation. This implies that the proposed model is conservative

$$\begin{aligned}
\delta^{hg}\Pi_{lin} &= \delta^{hg}\Pi_t \\
&+ \left(\frac{K}{V} - 2\frac{{}^{c}p_t}{v_t}\right) \int_\eta \int_\xi \Delta\mathbf{u} \cdot \ {}^{*}\mathbf{n}_t \ d\xi d\eta \int_\eta \int_\xi {}^{*}\mathbf{n}_t \cdot \delta\mathbf{u} \ d\xi d\eta \qquad \text{part I} \\
&+ \int_\eta \int_\xi \frac{{}^{x}p_t}{v_t} \ {}^{*}\mathbf{n}_t \cdot \Delta\mathbf{u} \ d\xi d\eta \int_\eta \int_\xi {}^{*}\mathbf{n}_t \cdot \delta\mathbf{u} \ d\xi d\eta \\
&+ \int_\eta \int_\xi {}^{*}\mathbf{n}_t \cdot \Delta\mathbf{u} \ d\xi d\eta \int_\eta \int_\xi \frac{{}^{x}p_t}{v_t} \ {}^{*}\mathbf{n}_t \cdot \delta\mathbf{u} \ d\xi d\eta \qquad \text{part II} \\
&- \frac{\rho_t}{2} \int_\eta \int_\xi \delta\mathbf{u} \cdot ({}^{*}\mathbf{n}_t \otimes \mathbf{g} + \mathbf{g} \otimes \ {}^{*}\mathbf{n}_t) \Delta\mathbf{u} \ d\xi d\eta \qquad \text{part III} \\
&+ \frac{1}{2} \int_\eta \int_\xi {}^{hg}p_t \begin{pmatrix} \delta\mathbf{u} \\ \delta\mathbf{u}_{,\xi} \\ \delta\mathbf{u}_{,\eta} \end{pmatrix} \cdot \begin{pmatrix} 0 & \underline{\mathbf{W}}^{\xi} & \underline{\mathbf{W}}^{\eta} \\ \underline{\mathbf{W}}^{\xi T} & 0 & \\ \underline{\mathbf{W}}^{\eta T} & 0 & 0 \end{pmatrix} \begin{pmatrix} \Delta\mathbf{u} \\ \Delta\mathbf{u}_{,\xi} \\ \Delta\mathbf{u}_{,\eta} \end{pmatrix} d\xi d\eta. \qquad (47) \\
&\qquad \text{part IV}
\end{aligned}$$

The different linearized parts can be interpreted as follows:

I The multiplication of the two surface integrals indicates the volume dependence of the compression level and of the pressure at the center of the fluid volume.

II The change of the local pressure is influenced by changes of the total volume and changes of the location of the center of the volume.
III A hydrostatic pressure generates a nonuniform pressure field, which is represented by a symmetric field equation under realistic boundary conditions, see [11], [12], [2].
IV Follower forces create a symmetric field equation too, considering realistic boundary conditions, see [11], [12], [2], [4], [13].

## 4 FE-Discretization and Solution Algorithm

The virtual work expression

$$\delta W = \delta^{el} V + \delta^{phg} \Pi - \delta^{ex} \Pi = 0 \tag{48}$$

followed by the linearization process as shown in chapter 3 leads to a residual and a linear term, depending only on the surfaces of the wetted resp. closed volumes. These terms have to be discretized with standard FE shell, membrane or continuum elements. Thus the boundary description is based on the surfaces of the FE elements wetted by the fluid or gas. Further, the discretized and linearized constraint equations as Hooke's law, the mass conservation of the fluid and the computation of the pressure at the center of the structure are included, resulting in general in a hybrid symmetric system of equations for the coupled problem:

$$\begin{bmatrix} {}^{el,phg}\mathbf{K} & -\mathbf{a} & -\mathbf{b} & \mathbf{a} \\ -\mathbf{a}^T & -\frac{K}{V} & 0 & 0 \\ -\mathbf{b}^T & 0 & -2\,{}^{c}pv & v \\ \mathbf{a}^T & 0 & v & 0 \end{bmatrix} \begin{pmatrix} \mathbf{d} \\ \Delta^k p \\ \frac{\Delta\rho}{\rho} \\ \Delta^c p \end{pmatrix} = \begin{pmatrix} {}^{phg}\mathbf{F} \\ 0 \\ 0 \\ 0 \end{pmatrix}. \tag{49}$$

This symmetric system can be reduced to a conventional symmetric displacement representation with the elastic and load stiffness matrix ${}^{el,phg}\mathbf{K} ={}^{el}\mathbf{K} +{}^{phg}\mathbf{K}$, the residual ${}^{phg}\mathbf{F}$ of internal ${}^{el}\mathbf{f}$, external ${}^{ex}\mathbf{f}$ and interaction forces ${}^{phg}\mathbf{f}$, the nodal displacement vector $\mathbf{d}$, a volume pressure gradient ${}^{phg}\alpha_t$ and two rank-one vectors $\mathbf{a}$ and $\mathbf{b}$

$$\begin{aligned} \left[{}^{el,phg}\mathbf{K} + \mathbf{b} \otimes \mathbf{a} + \mathbf{a} \otimes \mathbf{b}\right]\mathbf{d} &= {}^{phg}\mathbf{F} \\ &= {}^{ex}\mathbf{f} -{}^{phg}\mathbf{f} -{}^{el}\mathbf{f} \end{aligned} \tag{50}$$

This can be interpreted as a symmetric rank-two update of the matrix ${}^{el,phg}\mathbf{K}$ coupling all wetted degrees of freedom together. Applying the Sherman-Morrison formula an efficient solution can be computed by two additional forward-backward substitutions:

$$\mathbf{d}_1 ={}^{el,phg}\mathbf{K}^{-1}\,{}^{phg}\mathbf{F}, \quad \mathbf{d}_2 = {}^{el,phg}\mathbf{K}^{-1}\,\mathbf{a}, \quad \mathbf{d}_3 ={}^{el,phg}\mathbf{K}^{-1}\,\mathbf{b}. \tag{51}$$

The load stiffness matrix and the other pressure related terms are:

$$
\begin{aligned}
{}^{phg}\mathbf{K} = &-\frac{\rho_t}{2}\sum_e \int_\eta \int_\xi \mathbf{N}^T({}^*\mathbf{n}\mathbf{g}^T + \mathbf{g}\ {}^*\mathbf{n}^T)\mathbf{N}\ d\xi d\eta \\
&+\frac{1}{2}\sum_e \int_\eta \int_\xi {}^{phg}p_t \begin{pmatrix} \mathbf{N} \\ \mathbf{N}_{,\xi} \\ \mathbf{N}_{,\eta} \end{pmatrix}^T \begin{pmatrix} 0 & \underline{\mathbf{W}}^\xi & \underline{\mathbf{W}}^\eta \\ \underline{\mathbf{W}}^{\xi T} & 0 & 0 \\ \underline{\mathbf{W}}^{\eta T} & 0 & 0 \end{pmatrix} \begin{pmatrix} \mathbf{N} \\ \mathbf{N}_{,\xi} \\ \mathbf{N}_{,\eta} \end{pmatrix} d\xi d\eta,
\end{aligned}
\tag{52}
$$

$$
\mathbf{a} = \sum_e \int_\eta \int_\xi \mathbf{N}^T\ {}^*\mathbf{n}_t\ d\xi d\eta, \tag{53}
$$

$$
\mathbf{b} = \sum_e \int_\eta \int_\xi {}^{phg}\alpha_t \mathbf{N}^T\ {}^*\mathbf{n}_t\ d\xi d\eta, \tag{54}
$$

$$
{}^{phg}\mathbf{f} = \sum_e \int_\eta \int_\xi {}^{phg}p_t \mathbf{N}^T\ {}^*\mathbf{n}_t\ d\xi d\eta, \tag{55}
$$

$$
{}^{phg}\alpha_t = \frac{K}{2V} - \frac{{}^c p_t -{}^x p_t}{v_t}, \tag{56}
$$

$$
{}^{phg}p_t = {}^c p - {}^x p - {}^h p. \tag{57}
$$

The nodal displacement vector for one iteration step is then given by a linear combination of the three auxiliary solution vectors: $\mathbf{d} = \mathbf{d}(\mathbf{d}_1, \mathbf{d}_2, \mathbf{d}_3)$. For further details and the combination with arc-length schemes, we refer to [9] and [5]. For the cases pneumatics, hydraulics and incompressible fluids with open surfaces only a rank-one update is found. For pneumatics and hydraulics the pressure terms due to gravity disappear with ${}^c p ={}^x p = 0$, as well as the first term in ${}^{phg}\mathbf{K}$, as $g$ is not existent then. Depending on the pressure equation for gas or fluid

$$
{}^h\alpha_t = \kappa \frac{{}^k p_t}{v_t} \qquad \text{or} \qquad {}^h\alpha_t = \frac{K}{V} = \text{const.} \tag{58}
$$

and only a constant pressure term remains ${}^{phg}p_t = -{}^h p_t$.
For incompressible fluids ${}^{phg}\mathbf{K}$ has the same structure as for compressible fluids, but the pressure is dependent on the current coordinate of the fluid only ${}^{hg}p_t ={}^x p = \rho\mathbf{g}(-\mathbf{x}_t)$. However, we have to note that incompressibility can only be considered for fluids with open surfaces. For compressible fluids with open surface the pressure term ${}^h p$ due to overpressure is not present. Then the volume change due to the fluid weight is included in the ${}^c p$-term. However, in this case we have to keep also track of the current height of the fluid level, which is discussed in a forthcoming paper.

# 5 Numerical Examples

## 5.1 Pneumatic Multi-Chamber Structure Under Torsional Loading

A pneumatic multi-chamber structure see Fig. 1, two chambers with different initial internal pressure (left $p_{l0} = 0.01$ bar,right $p_{r0} = 1$ bar, with material

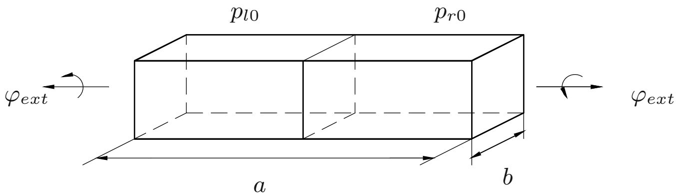


**Fig. 1.** Pneumatic multi-chamber system with flexible walls; loading by different initial internal pressure and torsion; geometrical data: $a = 10\ cm$, $b = 2\ cm$, $\varphi_{ext} = 45^o$, $p_{l0} = 0.01\ bar$, $p_{r0} = 1\ bar$

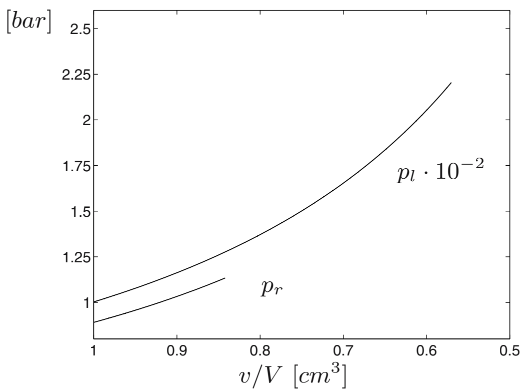


**Fig. 2.** Pneumatic multi-chamber system under torsional loading; internal pressure vs. relative volume change

law St.-Venant Kirchhoff, Young's modulus $E = 2.4 \cdot 10^4 \frac{N}{cm^2}$, Poisson ratio $\nu = 0.3$ and wall thickness $t = 0.1\ cm$ is first loaded with the different internal pressure. Then a torsional loading is applied by a rotation around the longitudinal axis by $\varphi_{ext} = 45^o$. In the FE model the nodes at one end are moved by prescribed displacements on circles in 20 equal sized steps. The chambers are discretized by 2300 solid-shell elements. The results of the analysis show the stiffening due to the internal pressure. The right chamber with high pressure is behaving like a rigid body, whereas the left chamber with low pressure is strongly deformed. The latter leads to a substantial increase of the internal pressure as a result of the volume reduction, see Figs. 2 and 3.

As the wall between both chambers is deformable, the pressure increase in the left chamber is also communicated to the right chamber resulting in a minor pressure increase there, too. In addition, we have to note that no stability problem arises during the deformation process; the dyadic extension due to the internal pressure somehow stabilizes the structure considerably and leads to a regularization of the equation system. The consistent linearization of the developed algorithm is visible in the quadratic convergence in the last

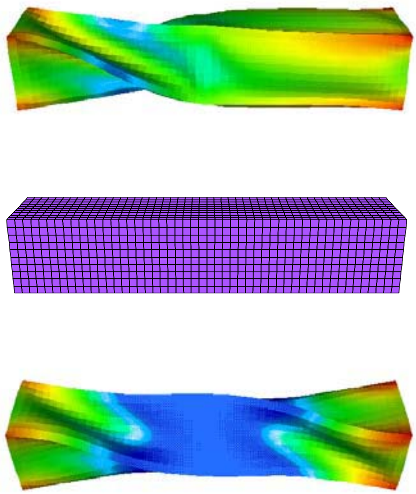


**Fig. 3.** Pneumatic multi-chamber system under torsional loading; (**a**) deformed high and low pressure chambers, (**b**) undeformed structure, (**c**) deformed structure without internal pressure

**Table 1.** Pneumatic multi-chamber system under torsional loading; convergence in the last load step at $\varphi_{ext} = 45^o$

| iteration step | 1 | 2 | 3 | 4 |
|---|---|---|---|---|
| energy | $7.09 \cdot 10^{+1}$ | $4.09 \cdot 10^{-1}$ | $2.49 \cdot 10^{-3}$ | $1.16 \cdot 10^{-4}$ |
| iteration step | 5 | 6 | 7 | 8 |
| energy | $3.52 \cdot 10^{-6}$ | $9.07 \cdot 10^{-8}$ | $2.09 \cdot 10^{-9}$ | $4.64 \cdot 10^{-11}$ |

iterations of the load steps. See e.g. the convergence behavior in the last load step at $\varphi_{ext} = 45^o$ in Table 1.

### 5.2 Hydrostatics of Partially Filled Multi-Chamber System with Interaction

This multi-chamber structure is chosen to show the effect of the interaction between fluid loaded chambers during a filling process. An open tank structure consisting of two deformable thin-walled chambers, separated by a thin wall is filled, see Fig. 4. Material law: St.-Venant Kirchhoff, Young's modulus $E = 2.0 \cdot 10^4 \frac{N}{cm^2}$, Poisson ratio $\nu = 0.3$, wall thickness $t = 0.1cm$, specific gravity of the fluid $\rho g = 0.1 \frac{N}{cm^3}$). The complete structure is modelled with 1100 solid-shell elements. In the first load step the left chamber is partially filled up to $w_{10}$ ($V_1 = 375cm^3$). Then the right chamber is filled with 30 equal sized volume steps of $\Delta V_2^* = 25\ cm^3$ starting with $w_{20} = 0$. In each load step the

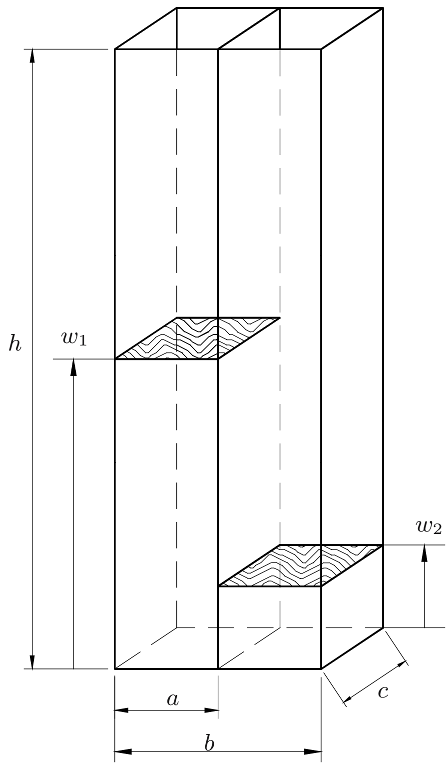


**Fig. 4.** Hydrostatics of multi-chamber system with interaction during filling; geometrical data: $a = 5cm,\ b = 10cm,\ c = 5cm,\ h = 30cm$

new filling height in the right chamber is determined via ${}^{o}x_2 ={}^{o} x_{t2} + \Delta u_2$ with $\Delta u_2 = \frac{V_2^*}{S_{t2}}$ using the free surface $S_{t2}$ computation. The chamber structure is deforming during the filling process and also the fluid level $w_1$ of the left chamber is rising as a result of the filling of the right chamber, see Figs. 5 and 6.

### 5.3 Elastic Cylindrical Vessel Fully Filled with Fluid

An elastic cylindrical vessel (weightless, elastic modulus $E = 21 \cdot 10^{10} \frac{N}{m^2}$, Poisson's ratio $\nu = 0.3$) with a very thin wall - close to a membrane - is completely filled with water (density $\rho = 1000 \frac{kg}{m^3}$, bulk modulus $K = 0.5 \cdot 10^9 \frac{N}{m^2}$). In a first load step the vessel is pressurized by 1 bar at the top of the vessel indicating the weight of the plate. In a second step the structure is loaded by a given displacement $u_{ext}$ of the loading plate, see Fig. 7b.

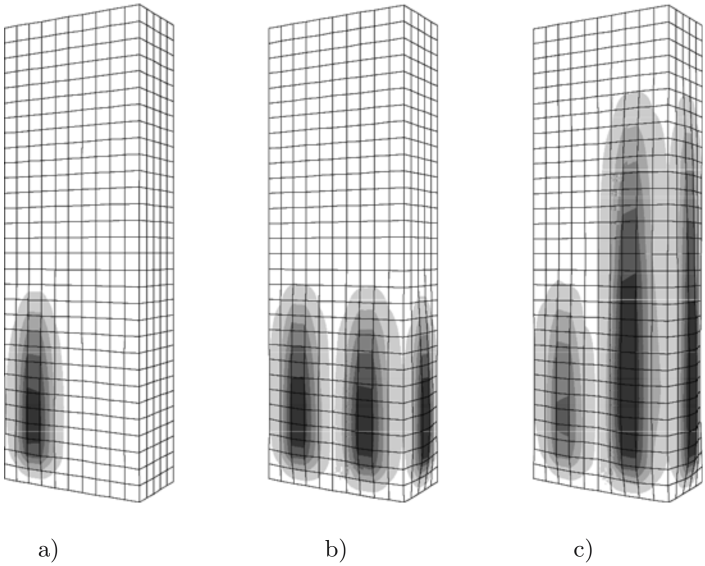


**Fig. 5.** Hydrostatics of multi-chamber system with interaction during filling; loading states: (**a**) left chamber filled up to $w_{10}$, right chamber empty, (**b**) right chamber partially filled and (**c**) after last load step (completely filled)

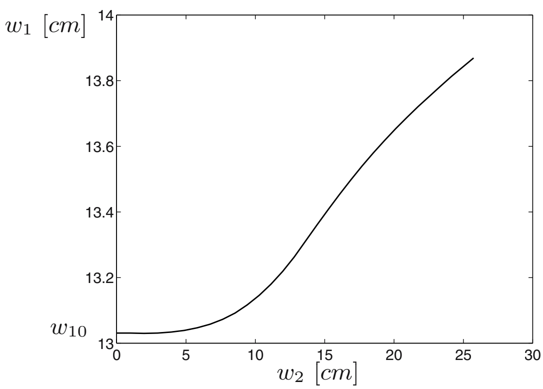


**Fig. 6.** Hydrostatics of multi-chamber system with interaction during filling; $w_{10}$ fluid level in left chamber before filling of right chamber; fluid level $w_1$ in left chamber versus fluid level $w_2$ in right chamber

Due to the deformation density and volume change according to the conservation of mass, see Fig. 8a. The decrease of the volume implicates an increase in the pressure level ${}^{h}p$ in the fluid. For comparison only a gas filling is con-

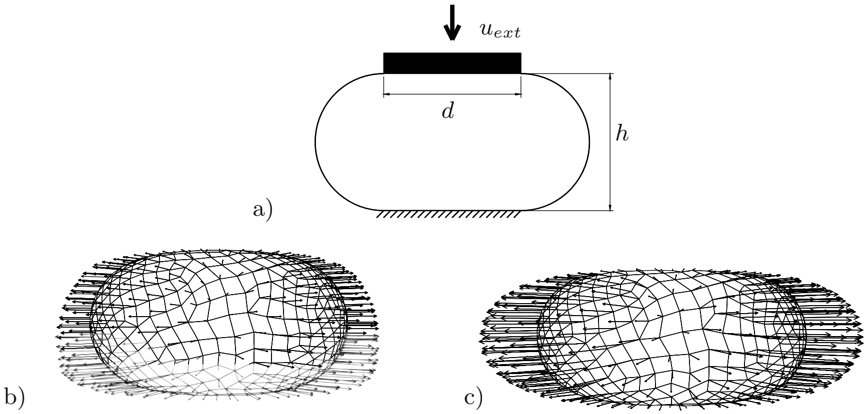


**Fig. 7.** Elastic cylindrical vessel fully filled (**a**) geometry and loading: height $h = 10m$, diameter $d = 10m$, piston displacement $u_{ext} = 4m$; (**b**) radial displacement vectors - first load step, (**c**) radial displacement vectors - final load step

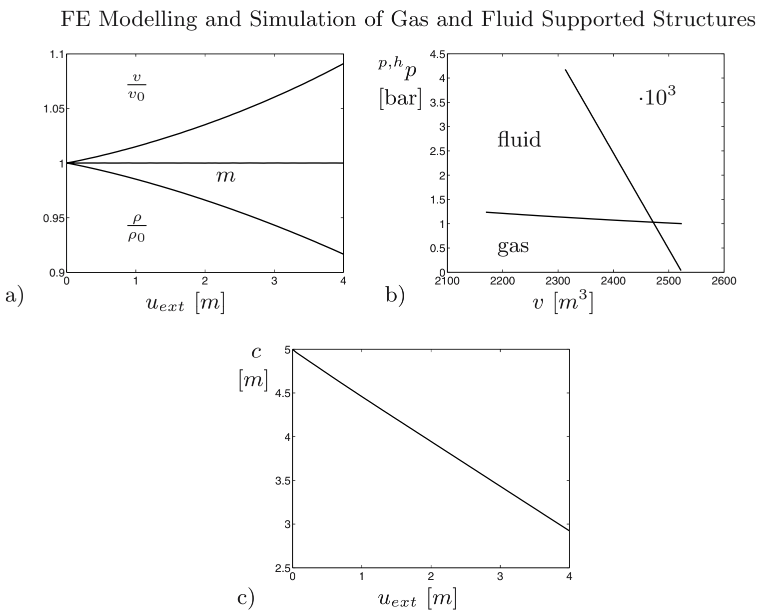


**Fig. 8.** Elastic cylindrical vessel fully filled (**a**) mass conservation vs. piston displacement $u_{ext}$, (**b**) fluid pressure $^{h}p$ / gas pressure $^{p}p$ vs. fluid volume $v$, (**c**) location of center $c$ of volume vs. piston displacement $u_{ext}$

sidered too, see Fig. 8b. A provisional result is the position of the center of the volume, which changes with the displacement of the piston, see Fig. 8c.

### 5.4 Fluid Filling of Strongly Deformable Thin-Walled Shell

In order to show the ability of the model to capture more numerically difficult situations the filling of a very thin-walled 2D-shell structure showing fairly large deformations almost similar to the deployment of membrane structures is chosen. The shell modelled with 8-node solid-shell elements is assumed to be weightless; material is of Neo-Hooke rubber type with elastic modulus $E = 9.6 \cdot 10^3 \frac{N}{m^2}$, Poisson's ratio $\nu = 0.3$, $t = 1mm$; the water is assumed to be incompressible, specific gravity of the fluid $\rho g = 0.01 \frac{N}{cm^3}$. The filling is performed via an external piston see Fig. 9.

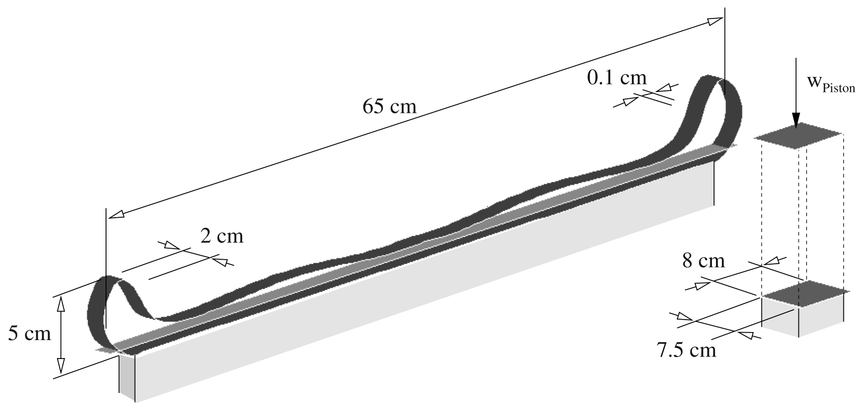


**Fig. 9.** Fluid filling of a strongly deformable shell, initial geometry and loading

A deformed situation is depicted in Fig. 10 with an almost filled structure. The shell is discretized with three different meshes of equal sized elements.

During the filling the water level is rising and touches the elements often only partially. As then the water pressure is checked at the Gauss-points of the surface (2*2 integration) convergence becomes difficult. In particular, when the load level comes into contact with the almost horizontal element faces, the number of iterations is rising, as minor changes in the water level lead to a major change in the wetted surface. As depicted in Fig. 11 the water level shows a rather linear dependence of the piston motion resp. the added water volume.

From the diagram in Fig. 12 we see that the algorithm allows a separation of the water surface without any problem which is more visible for the coarser mesh. The stiffer behavior of coarser mesh leads to a rather early separation whereas the finer meshes show a separation at an almost filled state, see e.g. Fig. 10. For a complete filling it would be necessary to take the compressibility of the water into account which is the subject of a forthcoming paper [9].

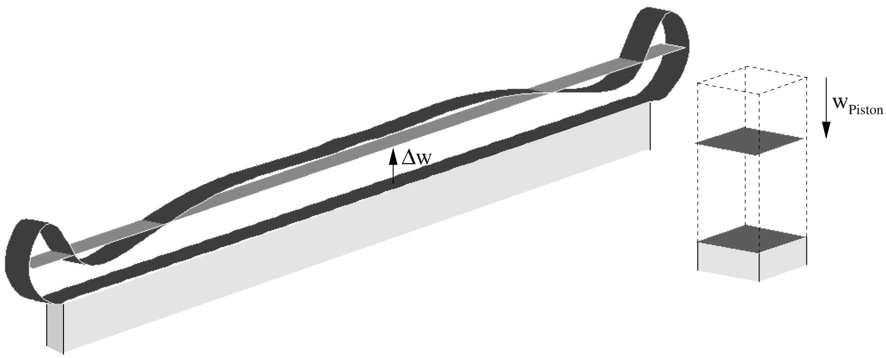


**Fig. 10.** Fluid filling of a strongly deformable shell; deformed state with almost fully filled structure

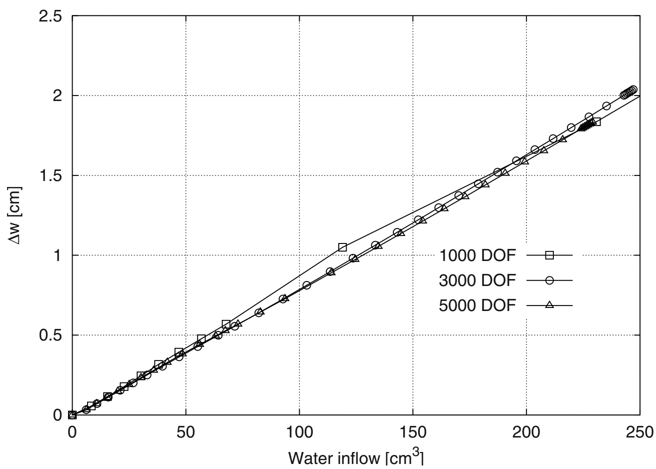


**Fig. 11.** Fluid filling of a strongly deformable shell; water level vs. added water volume

## 6 Conclusions

The proposed approach to describe the gas and fluid effects and their interaction with deforming structures by state equations has several advantages. First, the mesh-free modelling of the fluid resp. the gas allows to perform large deformation analysis without remeshing. Second, contact models between fluid and structure are not necessary. Third, stability investigations can be carried out taking the specific decomposition of the stiffness matrix

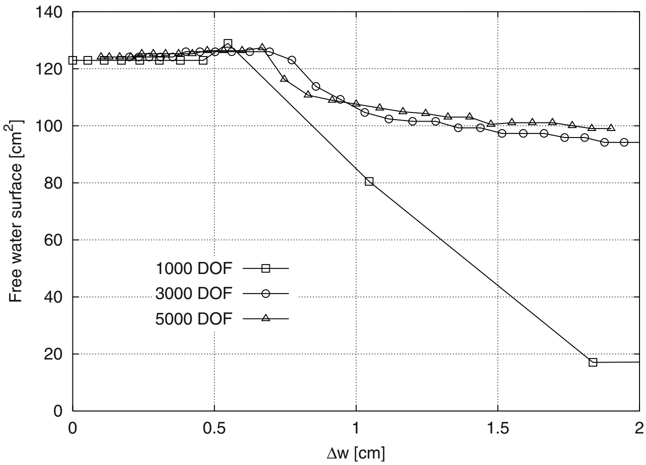


**Fig. 12.** Fluid filling of a strongly deformable shell; free water surface vs. water height

of the coupled problem into account, see [7]. Fourth, the solution of the coupled equation can be efficiently performed based on the subsequent use of the Sherman-Morrison formula involving only the triangular decomposition of the structural matrix. Summarizing all, the computational effort is significantly lower and better adjusted than in conventional methods based on full discretization. The numerical examples show the efficiency of the applications to thin-walled structures though due to the highly nonlinear behavior convergence is often rather difficult to achieve. Some of our forthcoming work is devoted to the static unfolding and filling of very flexible folded membrane like structures.

## References

1. J. Bonet, R.D. Wood, J. Mahaney, and P. Heywood. Finite element analysis of air supported membrane structures. *Comput. Methods Appl. Mech. Engrg.*, 190:579–595, 2000.
2. H. Bufler. Konsistente und nichtkonsistente druckbelastungen durch flüssigkeiten. *ZAMM*, 72(7):T172 – T175, 1992.
3. H. Bufler. Configuration dependent loading and nonlinear elastomechanics. *ZAMM*, 73:4 – 5, 1993.
4. G. Romano. Potential operators and conservative systems. *Meccanica*, 7:141–146, 1972.
5. T. Rumpel. *Effiziente Diskretisierung von statischen Fluid-Strukturproblemen bei grossen Deformationen.* Dissertation (in German), Universität Karlsruhe, 2003.

6. T. Rumpel and K. Schweizerhof. A hybrid approach for volume dependent fluid-structure-problems in nonlinear static finite element analysis. In J. Eberhardsteiner H.A. Mang, F.G. Rammerstorfer, editor, *Fifth World Congress on Computational Mechanics (WCCM V)*, 2002.
7. T. Rumpel and K. Schweizerhof. Volume-dependent pressure loading and its influence on the stability of structures. *Int. J. Numer. Meth. Engng*, 56:211–238, 2003.
8. T. Rumpel and K. Schweizerhof. Hydrostatic fluid loading in nonlinear finite element analysis. *Int. J. Numer. Meth. Engng*, 59:849–870, 2004.
9. T. Rumpel and K. Schweizerhof. Large deformation fe analysis of thin walled shell and membrane structures fully filled with compressible fluids. *(in preparation)*, 2004.
10. H. Schneider. *Flüssigkeitsbelastete Membrane unter großen Deformationen*. Universität Stuttgart, 1990. Dissertation.
11. K. Schweizerhof. *Nichtlineare Berechnung von Tragwerken unter verformungsabhängiger Belastung*. Universität Stuttgart, 1982. Dissertation.
12. K. Schweizerhof and E. Ramm. Displacement dependent pressure loads in nonlinear finite element analyses. *Computers & Structures*, 18(6):1099–1114, 1984.
13. M. J. Sewell. On configuration-dependent loading. *Arch. Rational Mech. Anal.*, 23:327–351, 1966.